Journal of proteome research

Cite This: J. Proteome Res. 2019, 18, 4027−4037

Article

pubs.acs.org/jpr

Proteome Integral Solubility Alteration: A High-Throughput Proteomics Assay for Target Deconvolution

Massimiliano Gaetani,[†,‡,#] Pierre Sabatier,[†,#] Amir A. Saei,[†,#] Christian M. Beusch,[†] Zhe Yang,[†] Susanna L. Lundström,[†,‡] and Roman A. Zubarev*[,†,‡,§]

[†]Division of Physiological Chemistry I, Department of Medical Biochemistry and Biophysics, Karolinska Institutet, SE-17 177 Stockholm, Sweden

[‡]SciLifeLab, SE-17 177 Stockholm, Sweden

[§]Department of Pharmacological & Technological Chemistry, I.M. Sechenov First Moscow State Medical University, Moscow, 119146, Russia

Supporting Information

ABSTRACT: Various agents, including drugs as well as nonmolecular stimuli, induce alterations in the physicochemical properties of proteins in cell lysates, living cells, and organisms. These alterations can be probed by applying a stability- and solubility-modifying factor, such as elevated temperature, to a varying degree. As a second dimension of variation, drug concentration or agent intensity/concentration can be used. Compared to standard approaches where curves are fitted to protein solubility data acquired at different temperatures and drug concentrations, Proteome Integral Solubility Alteration (PISA) assay increases the analysis throughput by 1 to 2 orders of magnitude for an unlimited number of factor variation points in such a scheme. The consumption of the compound and biological material decreases in PISA by the same factor. We envision widespread use of the PISA approach in chemical biology and drug development.

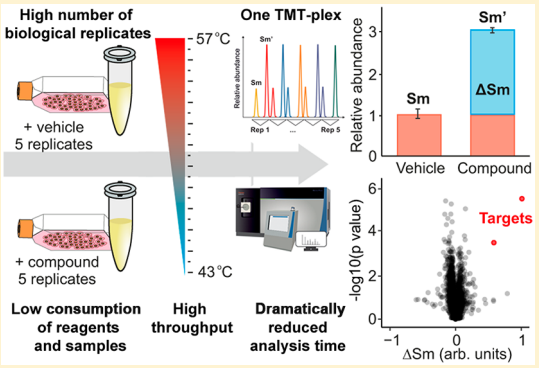

KEYWORDS: *target deconvolution, action mechanism, drug development, chemical biology, protein solubility, protein stability, high throughput, proteomics, mass spectrometry, tandem mass tag*

INTRODUCTION

Various agents, including drugs, nutrients, metabolites, and nonmolecular influences such as radiation, induce alterations in physicochemical properties of proteins in cell lysates, living cells, and organisms. These alterations can be probed on the proteome-wide scale by applying a stability- and solubility-modifying factor, such as temperature in thermal profiling,[1] proteolytic enzyme in partial proteolysis,[2,3] chaotropic agent in a solubility assay,[4] or salt in cation interaction profiling.[5] The factor is typically intensified in a stepwise manner, and then the proteins in soluble sample fractions—or alternatively the insoluble ones—are identified and quantified. The obtained information can be interpreted as drug binding to protein targets,[6,7] protein−protein docking, protein−small molecule interactions, and post-translational modifications.[8−11] As a prominent recent example, thermal proteome profiling (TPP),[1] translating the targeted approach of cellular thermal shift assay (CETSA)[12] onto a proteome-wide scale, can monitor protein stability and determine melting temperature shifts via changes in protein solubility with temperature. Temperature variations have long been applied to test the interactions of proteins with other molecules using fluorescence,[13,14] differential scanning calorimetry (DSC),[15,16] or mass spectrometry (MS)[17] as a readout. For instance, variations in signature thermograms of unfractionated plasma attributed to protein interactions with small molecules and peptides were monitored by DSC.[18] TPP is used not only for detecting protein−compound interactions,[19−22] but also for probing general protein stability;[23,24] determining changes of the internal environment in cells[8,9] and bacteria;[25] and identifying enzyme substrates.[11]

In 1D TPP, both drug-treated and untreated samples are incubated at several different temperature points (usually, $N_t \geq 10$). At each tested temperature, quantitative proteomics is then employed to measure the relative protein abundances. These are fitted by sigmoid curves, with melting temperatures T_m being calculated. The corresponding shifts ΔT_m induced by the drug are then determined (Figure 1a). To increase the analysis specificity, a second dimension is introduced, the drug concentration C. 2D TPP considers isothermal ΔT_m shifts as a function of C, from which C_0 (or pEC50[1]) are determined, which are the drug concentrations needed to induce half of ΔT_m.[1] Typically, the largest absolute ΔT_m values and the

Received: July 24, 2019
Published: September 23, 2019

DOI: 10.1021/acs.jproteome.9b00500
J. Proteome Res. 2019, 18, 4027−4037

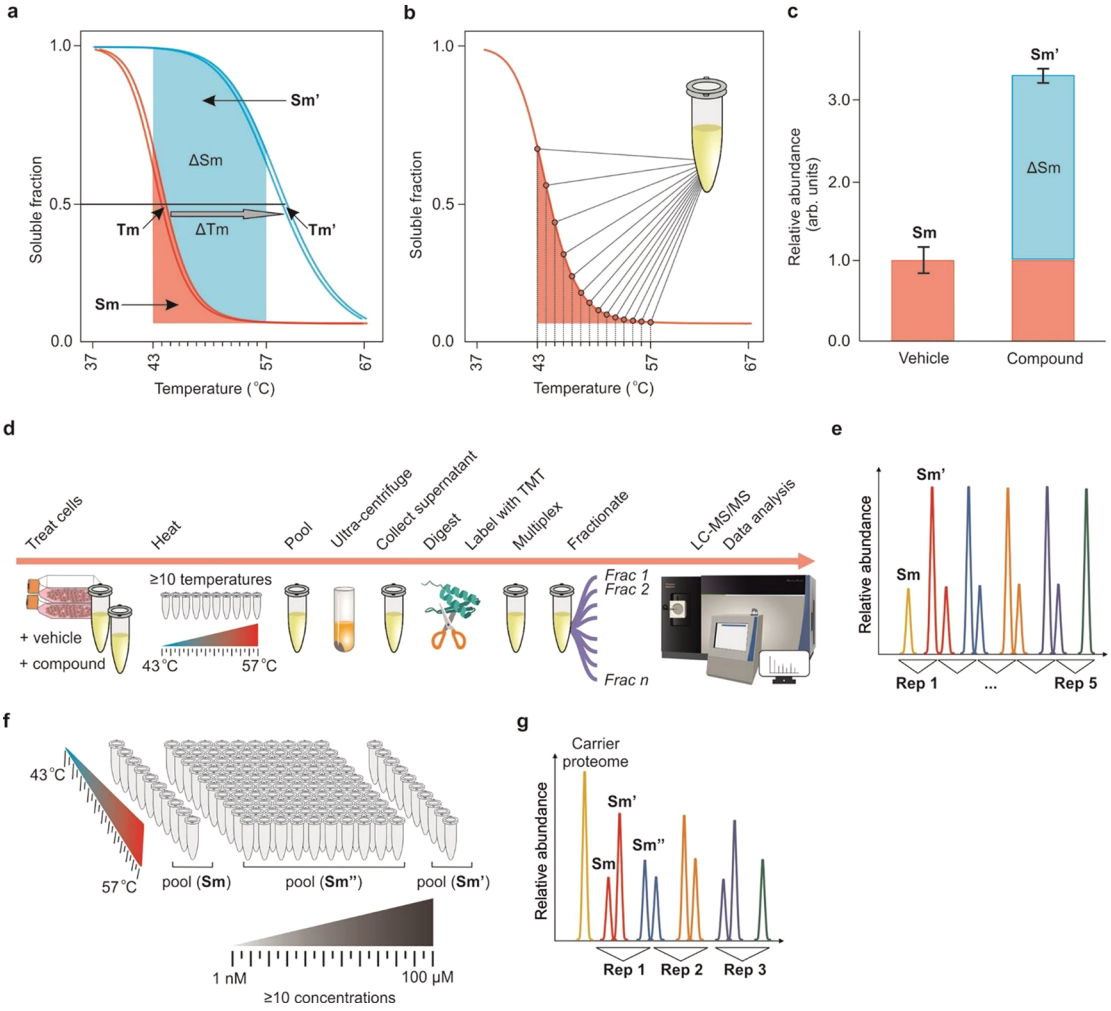

Figure 1. Schematics and workflow of PISA T. (a) Comparison of PISA concept of integral analysis with TPP concept of sigmoidal curve fitting: 1D PISA integral measurements of treated (blue area) and untreated (red area) sample for obtaining ΔS_m; 1D TPP - temperature scanning for treated (blue) and untreated (red) samples, curve fitting, and derived ΔT_m. (b) PISA T concept of pooling together individual samples corresponding to different temperature points and thus hardware integration of the melting curve without detailed determination of its shape. (c) Measuring ΔS_m as a difference between the integral abundances of the protein in the treated and untreated samples. (d) 1D PISA T experimental workflow, for each replicate sample: each sample is split in $N_t \geq 10$ equal parts, each part being heated at a different temperature. If cells are used, they are then lysed by freeze–thaw cycles. Then, the samples are pooled together before ultracentrifugation; the collected supernatant is then digested and TMT-labeled, which is followed by fractionation and LC-MS/MS analysis with subsequent data processing. (e) Example of a TMT-labeling scheme for five biological replicates of a 1D PISA T experiment. (f) 2D PISA T experimental workflow, including treatment with the compound over a series of concentrations. For each biological replicate, all concentration points different from zero and the highest one used are pooled together. Samples are otherwise processed as in 1D PISA T. (g) Example of a TMT-labeling scheme for three biological replicates of a 2D PISA T experiment, with one channel dedicated to the carrier proteome.

lowest C_0 values indicate the most likely drug targets or mechanistic proteins responding to the agent. This powerful approach is extremely resource consuming, often forcing one to reduce the number of parameter-scanning points to the detriment of specificity. A large number of cells is needed per replicate analysis—from 10^5 to 10^6 cells per scanned point, with a risk of different biological states being co-present in the cell population.[26] Curve fitting and extraction of T_m values are other important sources of experimental error. Although protein melting is considered a two-state transition from the folded native state to the random coil structure, intermediates often exist.[27,28] Due to protein solubility increase at lower temperatures, bimodal behavior, and other effects, single-transition sigmoidal curves can provide a poor fit for a large fraction of the proteome.[29] The nonparametric analysis of the TPP data is more robust than sigmoidal fitting,[30] but it is only a partial remedy for this generic problem. As a result, proteins with poorly fitted melting curves are discarded in TPP, which increases the risk of missing important targets or mechanistic proteins.

However, perhaps the most significant drawback of the traditional curve fitting method is its low throughput, while high-throughput phenotypic screening methods generate an ever-increasing number of hits that need to be validated. In order to increase the throughput of factor-probing proteomics approaches, we developed the Proteome Integral Solubility Alteration (PISA) assay which not only solves the above problems, but also achieves a dramatic reduction in both analysis time and sample consumption. We demonstrate these features by applying PISA with a temperature-based approach (PISA T), similarly to TPP.

DOI: 10.1021/acs.jproteome.9b00500
J. Proteome Res. 2019, 18, 4027–4037

EXPERIMENTAL PROCEDURES

Ab Initio Simulation

The simulation of sigmoidal curves of 1000 hypothetical proteins was carried out using the software *Excel* (Microsoft Office) and melting temperatures T_m selected randomly in the range from 42 to 57 °C. N_t = 16 temperature points between 37 and 67 °C with a 2 °C step were chosen. Sigmoidal melting curves were simulated by calculating the relative intensity $I(T)$ for a given temperature T as

$$I(T) = 0.5 + \mathrm{erf}[(T_m - T)/\mathrm{sqrt}(T_m)]/2 \quad (1)$$

where *erf* is the error function, and *sqrt* is the square root function.

The measured signal S_m was calculated as the sum of $I(T)$ values for all temperature points. ΔT_m were simulated as random values in the range between −5 °C and +5 °C, and T_m' values were calculated as $T_m' = T_m + \Delta T_m$. The corresponding melting curve intensities $I'(T)$ were calculated by (1) with T_m' being used instead of T_m. The S_m' values were obtained as the sums of all individual I' values. F_t values were obtained as

$$F_t = S_m' - S_m \quad (2)$$

The relative response $R(C)$ of the thermal protein solubility shift to different drug concentrations C was modeled as a somewhat steeper than temperamental sigmoidal curve

$$R(C) = 0.5 + \mathrm{erf}[2 \times (C_0 - C)/\mathrm{sqrt}(C_0)]/2 \quad (3)$$

where C is a given concentration point. $R(C)$ assumes values between 0 (very low concentrations) and 1 (very high concentrations). $R(C)$ assumes values between 0 (very low concentrations) and 1 (very high concentrations).

The measured readout S_m'' is a convolution of the temperature curve and the concentration curve. At zero drug concentration, the partial readout is equal to S_m, and at very high concentrations, it is equal to S_m'. For an intermediate case of the concentration C, the partial readout is $S_m + (S_m' - S_m) \times R(C)$. Integration over N_c concentration points gives the equation

$$S_m'' = N_c \times S_m + (S_m' - S_m) \times \mathrm{Sum}R_c \quad (4)$$

where N_c is the number of concentration points used and $\mathrm{Sum}R_c$ is the sum of the concentration responses (3) over N_c concentration points; we will denote it F_c. Experimentally, F_c can be derived from the measured values as

$$F_c = \mathrm{Sum}R_c = (S_m'' - N_c \times S_m)/(S_m' - S_m) \quad (5)$$

In order to simulate the TMT normalization necessary for data analysis, S_m, S_m', and S_m'' values were normalized such that the average value for each parameter over the whole data set is the same (e.g., 1). Consequently, the F_t formula for normalized parameters $S_m^{\#}$, $S_m'^{\#}$, and $S_m''^{\#}$ remains of the same form as eq 2

$$F_t \approx S_m'^{\#} - S_m^{\#} \quad (6)$$

while the formula for F_c changes to

$$F_c \approx (S_m''^{\#} - S_m^{\#})/(S_m'^{\#} - S_m^{\#}) \quad (7)$$

1D PISA T: Cell Culture and Temperature Treatment

Human lung carcinoma A549 and human kidney carcinoma A498 cell lines (ATCC, USA) were grown in at 37 °C in 5% CO_2 using, respectively, Dulbecco's Modified Eagle Medium (Lonza, USA) and RPMI 1640 medium (Gibco, Thermo Fisher Scientific, USA) supplemented with 10% FBS (Gibco, Thermo Fisher Scientific), 2 mM L-glutamine (Lonza), and 100 units/mL penicillin/streptomycin (Gibco, Thermo Fisher Scientific). Treatment of A549 cells with methotrexate (MTX) and of A498 cells with 5-fluorouracil (5-FU) was performed for 2 h in regular culture medium, while 15 min of incubation at room temperature was performed in the case of cellular lysates. Cellular lysates were obtained in phosphate buffered saline (PBS) supplemented with protease inhibitors (Roche, Switzerland) by four cycles of freezing cells in liquid N_2 and then thawing at 35 °C, then cleared by centrifugation at 10,000 *g* for 10 min at 4 °C. After cell detachment, each biological replicate was washed and suspended in PBS buffer supplemented with protease inhibitors (Roche), then split into equal portions for temperature treatment, which was performed for 3 min at each temperature using a SimplyAmp thermal cycler (Applied Biosystems, Thermo Fisher Scientific). Samples where then left at room temperature for 6 min before being snap frozen in liquid N_2. In the case of PISA in living cells, cells were lysed after thermal treatment and protein precipitation, by freezing and thawing cycles as described above. After the thermal treatment and protein precipitation at RT, equal aliquots of each temperature point were combined. Ultracentrifuge sedimentation of unfolded proteins was then performed at 150,000 *g* for 30 min at 4 °C using an Optima XPN-80 (Beckman Coulter, USA) ultracentrifuge.

Multidrug 1D PISA T

Human lung carcinoma A549 (ATCC) cells were grown until 80% confluence, and then cellular lysates were obtained in PBS as described above. These lysates were distributed into 10 equal aliquots and treated with each of the 9 drugs (nutlin, Tomudex, floxuridine, 8-azaguanine, topotecan, bortezomib, dasatinib, gefitinib, and vincristine) at a final concentration of 10 μM, as well as with the corresponding concentration of the dimethyl sulfoxide (DMSO) vehicle. Then each aliquot was distributed into 3 × 10 PCR tubes (triplicates) and thermally treated at 10 temperature points within a certain temperature range. Samples were then treated as described above for 1D PISA T.

2D PISA T

Human lung carcinoma A549 (ATCC) cells were grown until 80% confluence. Cells were harvested and a fraction of cells was lysed immediately using buffer composed of 1% SDS, 8 M urea, 50 mM Tris at pH 8.5, then sonicated with a probe sonicator (Branson Ultrasonics, USA) (10 times for 3 s plus 3 s on ice at 30% amplitude), followed by conventional shotgun proteomics sample preparation and TMT labeling (detergent-assisted proteome). The rest of the cells were lysed in PBS supplemented with protease inhibitors (Roche) by freezing–thawing, as described above. Each cellular lysate was distributed into 10 aliquots that were treated with 10 concentrations of MTX specified above. Then, each concentration point sample was distributed into 3 × 10 samples (technical triplicate) that were then heated at 10 different temperatures (43, 44.7, 46.4, 48.1, 49.8, 51.5, 53.2, 54.9, 56.6, and 58 °C). For each technical replicate treated at either the highest drug concentration or with drug vehicle only, aliquots of all temperature points were pooled as in 1D PISA T, while all temperatures of all remaining drug concentration points

DOI: 10.1021/acs.jproteome.9b00500
J. Proteome Res. 2019, 18, 4027–4037

were combined together in one pool. Samples were then treated as described above for 1D PISA T.

Proteomics Sample Processing

After measuring the total protein concentration by micro BCA assay kit (Thermo Fisher Scientific), 50 μg of each sample was reduced in 8 mM dithiothreitol (55 °C, 45 min) and alkylated in 25 mM iodoacetamide (25 °C, 30 min in darkness). This step was followed by protein precipitation using sample:cold acetone in a minimum ratio of 1:6 at −20 °C overnight. The precipitates were collected and washed with acetone by centrifugation (10 min, 10,000 g). Each dry pellet was first resuspended in 15 μL of 8 M urea in 20 mM 4-(2-hydroxyethyl)-1-piperazinepropanesulfonic acid (EPPS) buffer, and then 15 μL of 20 mM EPPS buffer containing 0.67 μg LysC enzyme (Wako, USA) was added (pH 8.2). The digestion with LysC was performed at 30 °C for 8 h. 90 μL of EPPS buffer containing 1 μg of sequencing grade modified trypsin (Promega, USA) was then added and the sample was digested overnight at 37 °C. 25 μg of each sample was labeled using TMT10 (Thermo Fisher Scientific) and ten samples were pooled into the final mixture (250 μg). Sample desalting and cleaning was performed using C18 (Sep-Pak, C18, Vac 1 cm^3, 50 mg, Waters, USA).

High pH Reversed Phase Fractionation

The peptides were separated using a Dionex Ultimate 3000 system (Thermo Scientific, Germany) on a Xbridge Peptide BEH C18 column (length, 25 cm; inner diameter, 2.1 mm; particle size, 3.5 μm; pore size, 300 Å; Waters) with a flow rate of 200 μL/min. Fractionation was applied using a binary solvent system consisting of 20 mM NH_4OH in H_2O (solvent A) and 20 mM NH_4OH in acetonitrile (solvent B). Peptides were eluted with a gradient from 2% to 23% B in 42 min, to 52% B in 4 min, to 63% B in 2 min, and then at 63% B for 5 min. The elution was monitored measuring UV absorbance at 214 nm. A total of 96 fractions of 100 μL each were collected and concatenated into 24 fractions.

LC−MS/MS Analysis

Each of the 24 fractions was analyzed by LC-MS/MS. Nano-high-performance liquid chromatography−electrospray ionization (HPLC-ESI)−MS/MS analyses were performed using a Q Exactive HF mass spectrometer (Thermo Scientific) equipped with an EASY Spray Source and connected to an UltiMate 3000 RSLC nanoUPLC system (Thermo Scientific). Injected sample fractions were preconcentrated and further desalted online using a PepMap C18 nano trap column (length, 2 cm; inner diameter, 75 μm; particle size, 3 μm; pore size, 100 Å; Thermo Scientific) with a flow rate of 3 μL/min for 5 min. Peptide separation was performed using an EASY-Spray C18 reversed-phase nano LC column (Acclaim PepMap RSLC; length, 50 cm; inner diameter, 2 μm; particle size, 2 μm; pore size, 100 Å; Thermo Scientific) at 55 °C and a flow rate of 300 nL/min. Peptides were separated using a binary solvent system consisting of 0.1% (v/v) formic acid (FA), 2% (v/v) acetonitrile (ACN) (solvent A) and 98% ACN (v/v), 0.1% (v/v) FA (solvent B) and eluted with a gradient of 4−26% B in 91 min, 26−95% B in 9 min. Subsequently, the analytical column was washed with 95% B for 5 min before re-equilibration with 4% B. Mass spectra were acquired in a mass-to-charge (m/z) range of 375−1500 with a resolution of 120,000 at m/z 200. Automatic gain control target was set to 3×10^6 with a maximum injection time of 100 ms. The 17 most abundant peptide ions were selected for higher-energy collision dissociation (HCD) with normalized collision energy value set at 33. The ion abundance threshold was set at 0.1% with charge exclusion of $z = 1$ ions. The MS/MS spectra were acquired at a resolution of 60,000, with a target value of 2×10^5 ions and a maximum injection time of 120 ms. The fixed first m/z was 100, and the isolation window was 1.6 m/z. The instrument was operated in the positive ion mode for data-dependent acquisition of MS/MS spectra with a dynamic exclusion time of previously selected precursor ions of 45 s.

Protein Identification and Quantitative Data Analysis

Protein identification and quantification was performed using MaxQuant v 1.6.2.3 using Andromeda as the search engine.[31] The complete Uniprot human proteome reference database (UP000005640) was applied for matching MS/MS spectra. TMT10 quantification of peptide and protein abundances was used. Cysteine carbamidomethylation was used as a fixed modification; methionine oxidation, arginine, and glutamine deamination were used as variable modifications for both identification and quantification. Trypsin/P was selected as enzyme specificity with maximum of two missed cleavages allowed. 1% false discovery rate was used as a filter at both protein and peptide levels. After removing contaminants, only proteins with at least two unique peptides were included in the final data set.

Quantification values for each protein were normalized on the total ion abundance of TMT10 reporters for a given protein and then on the average value for the untreated sample, to obtain the ΔS_m value. Two-tailed Student's t test (with equal or unequal variance depending on F-test) was applied to calculate p-values.

MS Proteomics Data Availability

The mass spectrometry proteomics data have been deposited to the ProteomeXchange Consortium via the PRIDE[32] partner repository with the data set identifier PXD013182.

RESULTS

PISA T Assay as an Alternative to Temperature and Concentration Scanning

In a 1D PISA T assay, two types of biological replicates are analyzed, with and without the agent (e.g., drug) applied. For each replicate, the protein mixtures are prepared for at least 10 (usually 15) individual temperature points N_t sampled at 1.0−1.5 °C intervals starting from 43 °C (Figure 1a). However, instead of labeling the trypsin digest of each of these samples by tandem mass tag (TMT) as in TPP, these protein mixtures are pooled together after thermal treatment (integral sample), as in Figure 1b. The aim of analysis is to measure the differences in the protein abundance in integral samples (Figure 1c). For that, the integral sample of each replicate is ultracentrifuged, digested, and labeled by a TMT (Figure 1d). Thus, a standard TMT-10 multiplexing scheme can combine 5 replicates for each of drug-treated and untreated samples (Figure 1e). After fractionation, the combined mixture can be analyzed by LC-MS/MS to a depth of >5000 proteins with an order of magnitude shorter instrumental time spent per replicate than in TPP.

In PISA T data processing, no curve fitting is performed to extract relative T_m; PISA T measures instead the protein abundance S_m in each integral sample. This abundance represents for each protein the integral of the area under its

DOI: 10.1021/acs.jproteome.9b00500
J. Proteome Res. 2019, 18, 4027−4037

melting curve within the used temperature interval, regardless of the actual curve shape (Figure 1a). If S_m is the readout for the untreated sample and S_m' is the corresponding value for the treated sample, then the PISA T analogue of ΔT_m is the function $F_t(S_m, S_m')$ that combines these two readout values. After proper normalization, the simplest form is $F_t = \Delta S_m = S_m' - S_m$ (Figure 1c), but we also found $F_t = S_m'/S_m$ to be useful, which has an advantage of not requiring normalization on the untreated sample. A TMT-10 labeling scheme affords five replicates of treated and untreated PISA T samples, e.g., S_m and S_m' (Figure 1e). These data will give rise to a volcano plot combining F_t with the p-values derived from the biological replicates, allowing one to select best candidate targets.

In a 2D PISA T assay, three samples are measured per replicate analysis (Figure 1f). The first two samples are the same as in 1D PISA T, i.e., one obtained without the drug and another with the maximum drug concentration. These two samples provide S_m and S_m' as readouts, from which F_t is obtained. The third sample is a pool of the protein mixtures where intermediate drug concentrations are used. The readout of this sample is the protein abundance S_m'', which represents an integral of the concentration-dependence curve. The analogue of TPP's readout C_0 is the function $F_c(S_m, S_m', S_m'')$.

The standard TMT-10 labeling set accommodates a 2D PISA T assay with three biological replicates plus an untreated proteome, which can be used for normalizing the S_m values (Figure 1g). The untreated proteome can be lysed with a detergent for enhanced protein extraction, which is avoided in TPP for the fear of affecting protein solubility in a nonlinear way.[29,33] This avoidance discriminates less soluble proteins, and thus curing this deficiency increases the depth of the proteome analysis, similarly to the carrier proteome in the single-cell proteomics approach.[34]

As shown below, S_m correlates well with the corresponding T_m extracted from sigmoidal melting curves; similarly, S_m' and T_m' values also correlate. Thus, from the S_m and S_m' data, one can extract the estimates of the T_m and T_m' values via modeling. Moreover, there is a good linear correlation between ΔT_m and F_t of any assumed sigmoidal curve. Similarly, there is a good linear correlation between C_0 and F_c. Therefore, in PISA, the information on these parameters in not lost, and if needed can be derived through modeling.

Ab Initio Simulation of PISA

As a theoretical proof of principle, we simulated 1000 sigmoidal curves for T_m in a 42−57 °C range using error (*erf*) and square root (*sqrt*) functions. Examples of thus-simulated melting curves are shown in Figure 2a (more details in Experimental Procedures). When separately sorted by T_m and S_m, the protein ranks were found to be equal, validating the hypothesis that S_m is a suitable proxy for T_m. The drug-induced melting temperature shifts ΔT_m were simulated within the range of −5 to +5 °C, yielding S_m'. The $F_t = S_m' - S_m$ values showed an excellent correlation with the corresponding ΔT_m values (Figure 2b, $R^2 > 0.998$), proving the linear function to be a suitable approximation. Knowing the regression parameters, the model T_m value can be derived from the measured S_m data.

The relative response $R(C)$ of protein solubility to variation of drug concentrations C was also modeled (Figure 2c). The measured readout S_m'' is a convolution of the temperature curve and the concentration curve. At zero drug concentration, the readout is equal to S_m, and at a maximum concentration, it is equal to S_m'. For an intermediate concentration C, the readout is $S_m + (S_m' - S_m) \times R(C)$. Integration over n concentration points gives $F_c = \mathrm{Sum}R_c$. In our simulations, F_c strongly correlated with $-\log10(C_0)$ ($R^2 \approx 0.999$, Figure 2d). Thus, F_c can be a proxy for the threshold concentration. Using linear regression, it is possible to extract the model C_0 values from experimental PISA data.

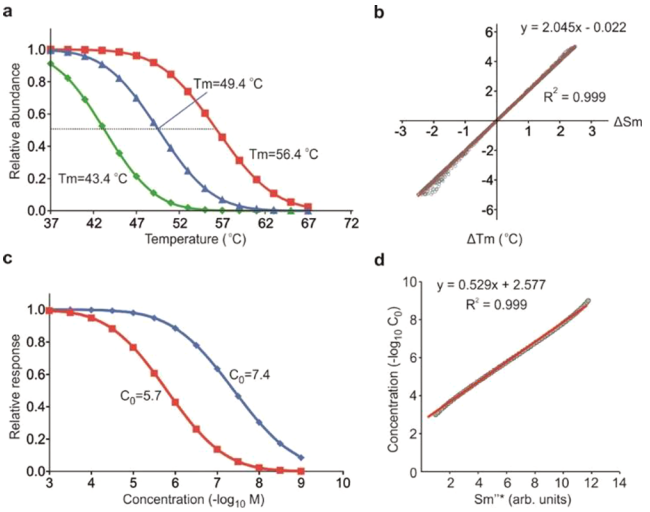

Figure 2. *Ab initio* simulation of 2D PISA T. (a) Simulated melting curves. (b) Correlation between the simulated $F_t = S_m' - S_m$ and ΔT_m values. (c) Simulated response of the thermal protein stability/solubility shift to different drug concentrations. (d) Correlation between the calculated S_m''* values and C_0 concentration.

Experimentally TMT-derived relative abundances need to be normalized because of various factors affecting the sensitivity of different TMT channels. In our simulations, S_m, S_m', and S_m'' values are normalized to $S_m^{\#}$, $S_m'^{\#}$, and $S_m''^{\#}$ to have equal average value for each parameter over the whole data set (e.g., 1). While the F_t formula remains the same as before normalization retaining a very high ($R^2 \approx 0.999$) correlation with ΔT_m, the formula for F_c changes with normalization, producing a correlation with $-\log10(C_0)$ that is somewhat reduced ($R^2 > 0.89$ for ranks), but still sufficiently high for most practical purposes.

These simple *ab initio* simulations provided theoretical proof of principle for the 2D PISA T method.

Simulation of 1D PISA T Output from Experimental TPP Results

An additional proof of principle for PISA was performed through the analysis of published TPP data via simulation of the PISA readout. Using the TPP data sets where cells and cell lysates were treated with dasatinib,[1] S_m and S_m' were calculated as the sums of protein abundances at all temperature points between 41 and 59 °C (Table S1 and Table S2). The average correlation between the two replicates of the ΔT_m values of the proteins surviving the stringent TPP filters for curve fitting was 0.903, while the average correlation between the corresponding ΔS_m values was 0.946. This corresponds to a higher precision of the S_m calculation compared to curve fitting in TPP. As a result, using the same statistical criteria for significance, there were 259 significant proteins in PISA analysis of cells and lysates, a 3% increase compared to 251 significant proteins in TPP (Figure 3a,b and d,e, respectively). At the same time, there was an excellent correlation between the replicate-averaged ΔT_m and ΔS_m values, $R = 0.947$ for cells and $R =$

DOI: 10.1021/acs.jproteome.9b00500
J. Proteome Res. 2019, 18, 4027−4037

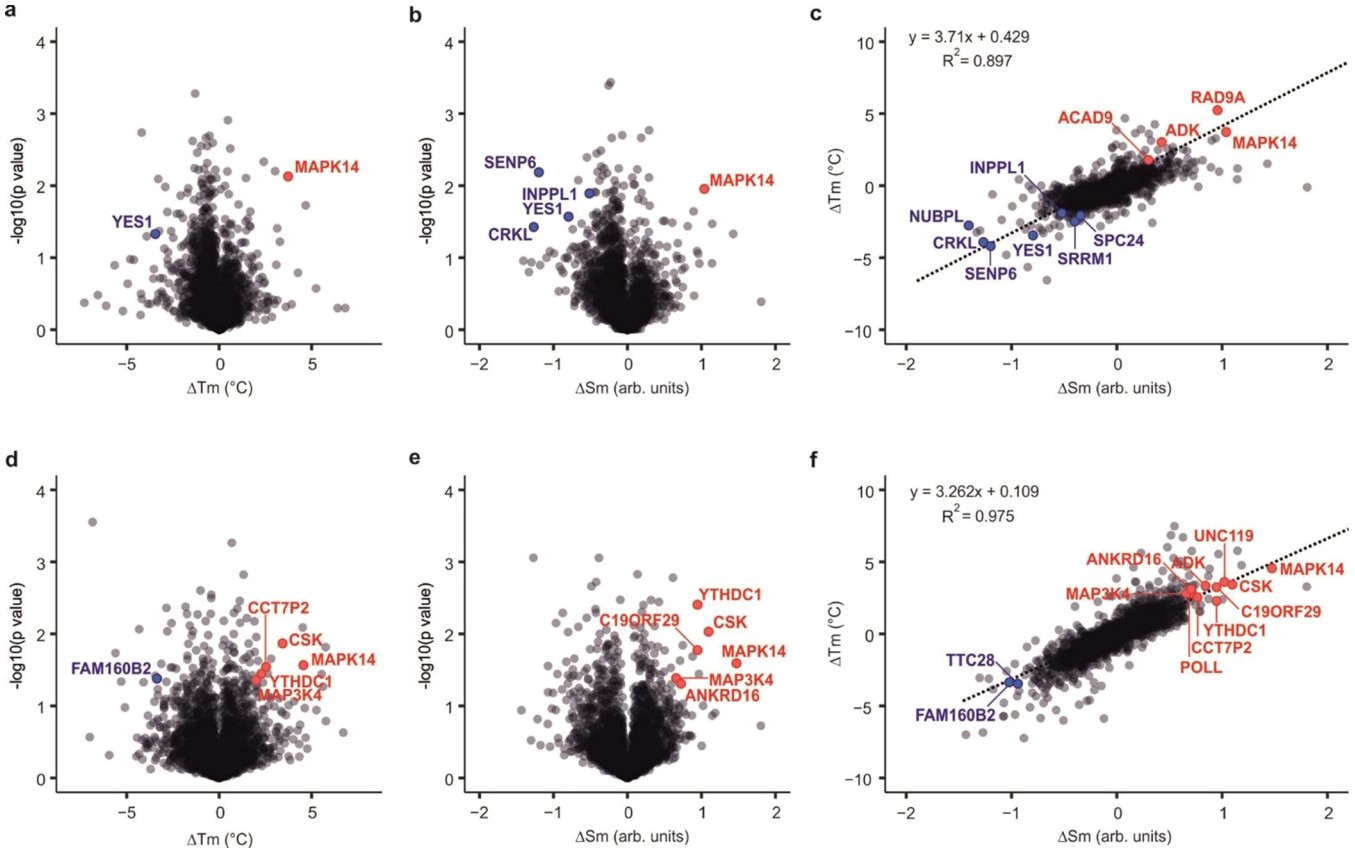

Figure 3. Simulation of 1D PISA T data analysis based on published TPP data sets. In all panels, proteins passing all four cutoff filters of TPP are indicated by red (stabilized) or blue (destabilized). (a) Volcano plot (ΔT_m, p) for TPP data of 5 μM dasatinib treatment of cells. (b) Corresponding volcano plot (ΔS_m, p) of the calculated PISA results. (c). Correlation between the average ΔT_m and average ΔS_m values for treatment of living cells with dasatinib. (d–f) Same as (a–c) for cell lysates, respectively. Data are extracted from the proof of principle article published on TPP.[1]

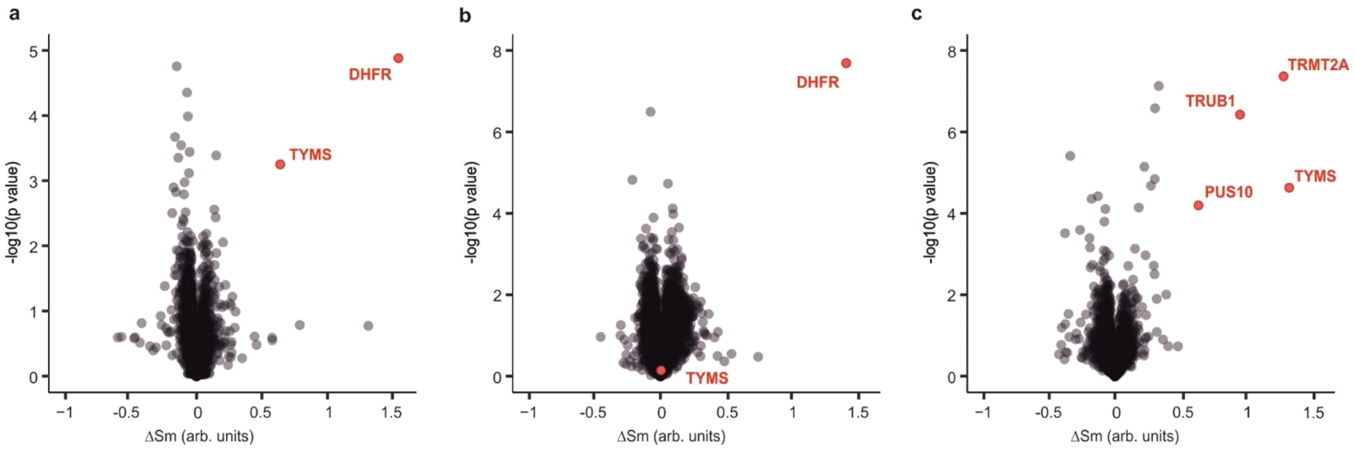

Figure 4. 1D PISA T results for different compounds in cells and lysate. Known identified targets are shown in red and labeled. (a) A549 cells treated with MTX. (b) A549 cell lysates treated with MTX. (c) A498 cells treated with 5-FU.

0.987 for lysates (Figure 3c and f, respectively). These correlations were actually higher than that those between the two ΔT_m replicates in the original data sets, which were R = 0.849 and R = 0.931 for cells and lysates, respectively.

Experimental 1D PISA T Assays on Methotrexate and 5-Fluorouracil

For experimental proof of principle, PISA T was performed on two cell lines, lung carcinoma A549 and kidney carcinoma A498, using two drugs with well-known targets. We used the folate and nucleoside analogs MTX and 5-FU, known to inhibit, respectively, dihydrofolate reductase (DHFR), involved in the tetrahydrofolate synthesis, and thymidylate synthetase (TYMS), key enzyme in *de novo* synthesis of thymidylate.[35−39] These drugs and their targets have been subjects of studies using antibody-based targeted protein detection in CETSA, with the targets showing increased stability/solubility after drug incubation.[40,41] These drugs are frequently used in proof of principle experiments in developing

DOI: 10.1021/acs.jproteome.9b00500
J. Proteome Res. 2019, 18, 4027−4037

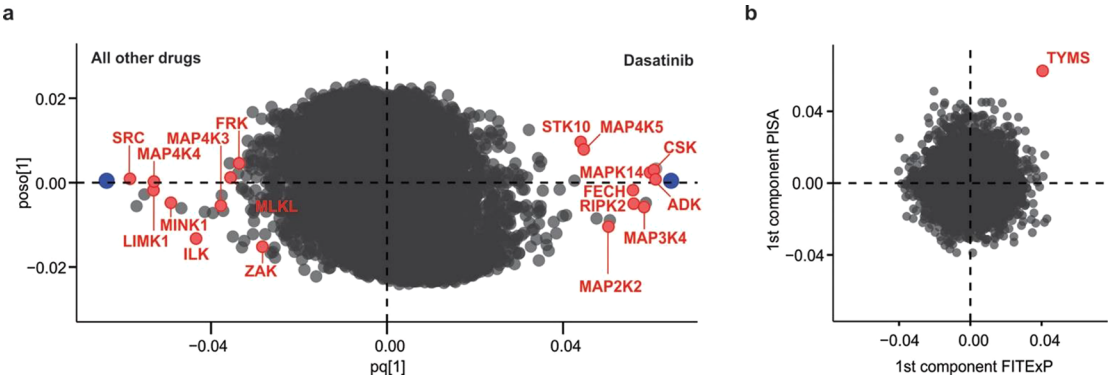

Figure 5. Results of multidrug 1D PISA T. (a) OPLS-DA plot of dasatinib data contrasted with all treatments, except gefitinib. Known targets (kinases) are shown in red. (b) Comparison of FITExP results with PISA assay data on Floxuridine treatment for the 5599 common proteins. The Floxuridine target TYMS shows most elevated specific expression as well as highest positive stabilization.

novel target deconvolution approaches, e.g., Functional Identification by Expression Proteomics (FITExP),[42] a proteome-wide strategy orthogonal to TPP.

As a first step of analysis, IC_{50} values of MTX in A549 cells and 5-FU in A498 cells were measured, as in specific experimental settings the results frequently deviate from the literature data. Resulting values were 1.0 μM for MTX in A549 and 17.5 μM for 5-FU in A498 cells. Drug concentration corresponding to 5 times the IC_{50} value was used in treatments, with vehicle as a control. Experiments on both cells and cell lysates were performed in 5 biological replicates. Proteins were treated at N_t = 15 temperature points, after which the aliquots were allowed to precipitate at room temperature and pooled together. When living cells were treated, cell lysis was performed before pooling the samples. Ultracentrifugation was used to pellet down and exclude the protein insoluble fraction. Digestion and TMT10 labeling was followed by fractionation. LC-MS/MS shotgun proteomic analysis provided protein identification and relative quantification.

For MTX in A549 cells, both DHFR and TYMS were strong positive outliers in the ΔS_m distribution (Figure 4a, Table S3). In the corresponding cell lysate, only DHFR was an outlier (Figure 4b, Table S4), confirming DHFR as the primary target of MTX and TYMS as a secondary target after molecule metabolism in living cells. Similar results were obtained for 5-FU that acts through its metabolites.[43] While in A498 living cells, the major target candidates are clear outliers (Figure 4c, Table S5), in cell lysates their ΔS_m values were not significant (Figure S1 and Table S6). These proteins were as follows: TYMS, the well-known target of 5-FU;[44] tRNA (uracil-5-)-methyltransferase (TRMT2), a member of tRNA modifying enzymes discovered as targets of 5-FU and mediators of its toxicity;[45] TRUB1 and PUS10, pseudouridine synthases known to form complexes with 5-FU.[46−49] In addition to the TYMS pathway, proteins with highly reproducible $\Delta S_m > 0.1$ showed interconnection within pathways involving pseudouridine synthesis (7 proteins, FDR = 5.37×10^{-15}), RNA modification (9 proteins, FDR = 6.55×10^{-14}), and ribosome biogenesis (3 proteins, FDR = 1.79×10^{-2}) (Figure S2). Of note, only when the depth of the proteome analysis exceeded 5000 proteins, PISA assay identified candidates other than TYMS, highlighting the importance of deep proteome analysis in drug target discovery.

1D PISA T in a Multidrug Approach

To capitalize on the unique analytical power of PISA due to sample volume reduction, we treated A549 cell lysates with 9 drugs (nutlin, Tomudex, floxuridine, 8-azaguanine, topotecan, bortezomib, dasatinib, gefitinib, and vincristine) previously used in a deep-proteome FITExP analysis.[11] We used three biological replicates for each drug and vehicle-only control. The complete 1D PISA T analysis lasted less than a week of MS instrumental time, while with TPP the same effort would require between two and three months, an enterprise prohibitive for most research groups in terms of cost and failure risks. The analysis yielded 6926 proteins quantified across all replicates without missing values and at least two peptides (Table S7). To this data set we applied the specificity concept previously used only in FITExP, ProTargetMiner, and SIESTA[11,39,50,51]—namely, contrasting for every protein by Orthogonal Partial Least Squares-Discriminant Analysis (OPLS-DA) the ΔS_m value obtained for any particular drug against those for all other drugs. As an example, the treatment by the kinase inhibitor dasatinib showed as major target candidates several kinases including the targets listed in DrugBank (SRC, MAPK14, CSK, FRK, and ZAK) as well as FECH that is a common off-target of kinase inhibitors[52] (OPLS-DA coordinates in Table S8). As gefitinib has similar targets, it was removed from the data set when contrasting with dasatinib, which increased the analytical specificity (Figure 5a). Moreover, by using 1D PISA T in a multidrug approach we were able to test nine drugs in triplicate with an experimental expenditure at least 25% lower than testing just one single drug in duplicate by TPP. This design has 10−20 times throughput increase compared to TPP and the advantage of being able to extract drug specific signatures via OPLS-DA multivariate analysis. As consequence of a multidrug approach, the resulting data set is larger and more complex; however, the gain well justifies the increase in data complexity using this experimental design.

We were able to compare for the first time the target specific expression in FITExP with the thermal solubility change in 1D PISA T for the 5599 proteins common in both data sets and proved the orthogonal nature of these two approaches. This experiment will be discussed in detail elsewhere; here, we note that the primary target of Floxuridine, TYMS, was identified as an outlier in both types of analysis (Figure 5b, OPLS-DA coordinates in Table S9).

DOI: 10.1021/acs.jproteome.9b00500
J. Proteome Res. 2019, 18, 4027−4037

2D PISA T

For the experimental proof of principle of 2D PISA T, A549 lysate was treated with MTX. Ten temperature points in the range from 43 to 58 °C and N_c = 10 concentration points (vehicle only, 1 pM, 10 pM, 100 pM, 1 nM, 10 nM, 100 nM, 1 μM, 10 μM, 100 μM) were used. One TMT10 channel was used for the detergent-lysed untreated proteome, while the remaining TMT10 channels hosted three biological replicates of 2D PISA samples (Figure 1g). Treatments with MTX were performed on equal volumes of cell lysates as described for 1D PISA T, and then each sample was separated into 10 aliquots incubated at different temperatures. For samples treated with the vehicle only, as well as the highest drug concentration, temperature points were pooled together as in 1D PISA T, to provide S_m and S_m' measurements. The 8 intermediate concentrations were separated into 10 temperature aliquots. After drug and thermal treatment, all 80 aliquots of each replicate were pooled together, to provide the S_m'' measurement. In total, 7427 proteins were quantified in all three replicates without missing values (Table S10). The abundances of proteins were normalized as described, and then F_t and F_c parameters were calculated. The F_t and F_c values in general correlated very poorly (R^2 < 0.13), confirming that these two parameters are largely independent of each other, thus providing a truly two-dimensional data set.

There were only seven significant (E < 0.05) proteins for F_t, with DHFR having both the highest value and highest significance (E < 0.002). Similarly, only 11 proteins were significant for F_c values, with DHFR being the only protein among these with a significant F_t. Thus, DHFR was identified with 2D PISA T as the sole target for MTX in lysate. This proved the principle of 2D PISA T (Figure 6).

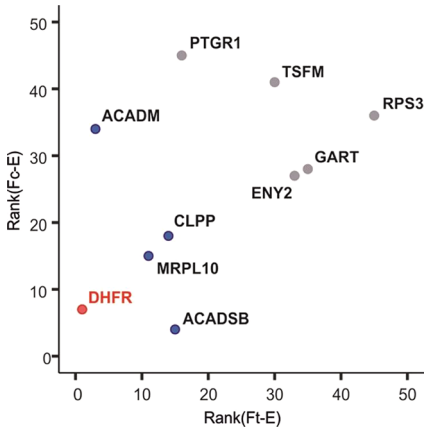

Figure 6. 2D plot of the significance ranks for F_t and F_c in 2D PISA T. The top protein exhibiting the highest F_t value among all proteins is shown in red. Mitochondrial proteins are shown in cyan blue.

Interestingly, among the 11 F_c-significant proteins, two molecules related to DHFR by function: C-1-tetrahydrofolate synthase and 5-formyltetrahydrofolate cyclo-ligase. Additionally, mitochondrial short/branched chain specific acyl-CoA dehydrogenase belongs to the family of proteins upregulated by MTX at the mRNA level (http://www.t3db.ca/toxins/T3D2486, Supporting Information). These results show that the F_c dimension of 2D PISA T added information on biological relevance to F_t analysis.

Supporting the tentative interaction of acyl-CoA dehydrogenases with MTX, one of the seven F_t-significant proteins is mitochondrial medium-chain specific acyl-CoA dehydrogenase ACADM. Another molecule in that list is the mitochondrial acyl carrier protein NDUFAB1. Overall, in the list of proteins sorted by their E-value ranks for F_c and F_t, the top protein is unquestionably DHFR, followed by five mitochondrial proteins (Figure 6). Finally, DHFR could be verified by 2D PISA T as the protein combining the highest solubility alteration with action at a low drug concentration, as would be expected for a true target.

DISCUSSION

The specificity increases in PISA T compared to TPP can come from three sources. First, the use of a larger *number* of temperature points N_t comes at no additional cost in terms of LC-MS/MS instrumental time. Larger N_t within the same temperature *range* means reduction of errors associated with discrete measurements, and more accurate capture of the various types of protein melting behaviors. The use of higher N_t can also mitigate the error arising due to statistical noise, e.g., single point outliers. When N_t = 20 were tested, p-values for known target proteins were lower than with N_t = 10. Of relevance, the dynamic range of the PISA T readout can be increased by narrowing the temperature range to the region of the most significant solubility changes, excluding both the low- and high-solubility plateau that are crucial for TPP curve fitting but are unimportant in PISA.

The second reason for increase of specificity in PISA T compared to TPP is that the integral under the melting curve S_m is statistically more robust than the derived curve-fitting parameters, which are subjects to various statistical uncertainties. The complicated TPP data analysis requiring fitting of full melting curves and applying complex statistics is reduced in PISA to a much simpler quantitative data analysis using relative protein abundances and p-values of their changes. For this reason, PISA T also allows one to measure behavior of proteins otherwise lost in TPP due to curve fitting errors. Additionally, all the procedures downstream from temperature treatment, such as reduction/alkylation, digestion, and TMT labeling, are performed on a single pooled sample, reducing the experimental errors and thus improving the p-values.

The third reason is the larger number of biological replicates that can be analyzed in practice compared to TPP that is commonly performed only in biological duplicates.[29] The increase of number of replicates in TPP would require the corresponding increase in experimental costs, particularly in instrument time. In 1D PISA T, five-replicate experiments can be performed at the cost of a single TMT-10 analysis, exactly half the amount of time of a single TPP replicate. The statistical power derived from five-replicate experiments in PISA T allows one to identify with high significance even proteins with tiny thermal shift, which are more difficult with the curve fitting approach.[11]

For an equal number of replicates, the throughput in 1D PISA T is increased by a factor of N_t compared to TPP, while in 2D PISA T the theoretical increase is $N_t \cdot N_c$, possibly reaching 2 orders of magnitude when both N_t and N_c are on the order of 10. 2D PISA T is also capable, at the sole cost of one 10-plex analysis, to test in triplicate putative multitarget compounds in cellular lysates and determine the hierarchy between the targets based on the solubility change at a lower compound concentration. The reduction of experimental

DOI: 10.1021/acs.jproteome.9b00500
J. Proteome Res. 2019, 18, 4027−4037

expenditure and the increase in sensitivity are both by a factor of N_t compared to TPP. In drug discovery, where an experimental drug can have high cost, PISA offers substantial cost reduction. In SIESTA,[11] where the cost of a purified, active recombinant enzyme can be dominant, the benefit of using PISA instead of TPP will be especially appreciable.

The main concept of PISA, which is the use of the integral under the curve instead of the curve shape parameters, is suitable for analytical methods where curve fitting is employed to probe protein stability or solubility perturbed by various agents. These methods include limited proteolysis combined with MS,[53] the use of urea or other chaotropic agents,[4] pressure, pH at high (or low) values, or high (or low) salt concentrations.[5]

■ ASSOCIATED CONTENT

Supporting Information

The Supporting Information is available free of charge on the ACS Publications website at DOI: 10.1021/acs.jproteome.9b00500.

Figure S1. 1D PISA T results for 5-FU in A498 cell lysate. Figure S2. 5-FU action mechanism by 1D PISA. (a) Volcano Plot of 1D PISA T for 5-FU in A498 cells. (b) STRING analysis of proteins with significant ΔS_m > 0.1. (PDF)

Table S1. Simulation of 1D PISA T output from published TPP results for dasatinib in cells. (XLSX)

Table S2. Simulation of 1D PISA T output from published TPP results for dasatinib in cell lysate. (XLSX)

Table S3. 1D PISA T for MTX in A549 cells. (XLSX)

Table S4. 1D PISA T for MTX in A549 cell lysate. (XLSX)

Table S5. 1D PISA T for 5-FU in A498 cells. (XLSX)

Table S6. 1D PISA T for 5-FU in A498 cell lysate. (XLSX)

Table S7. Multidrug 1D PISA T. (XLSX)

Table S8. OPLS-DA coordinates for dasatinib against all other drugs (excluding gefitinib). (XLSX)

Table S9. OPLS-DA coordinates for floxuridine in multidrug 1D PISA T versus FITExP. (XLSX)

Table S10. 2D PISA T for MTX in A549 cell lysate. (XLSX)

Supporting T3D2486.zip archive. Hard copy of the webpage http://www.t3db.ca/toxins/T3D2486 (ZIP)

■ AUTHOR INFORMATION

Corresponding Author

*E-mail: roman.zubarev@ki.se.

ORCID

Massimiliano Gaetani: 0000-0001-5610-0797
Pierre Sabatier: 0000-0002-2734-1791
Roman A. Zubarev: 0000-0001-9839-2089

Author Contributions

#M.G and R.A.Z. designed the research. M.G., P.S., Z.Y., and S.L.L., performed experiments. M.G., P.S., A.A.S., C.M.B., Z.Y., S.L., and R.A.Z. analyzed the data. M.G., P.S., and R.A.Z. wrote the paper. All authors have given approval to the final version of the manuscript. M.G., P.S., and A.A.S. contributed equally.

Notes

The authors declare no competing financial interest.

■ ACKNOWLEDGMENTS

All experiments were performed as method development of the Chemical Proteomics Core Facility (CPCF) located at Biomedicum, Karolinska Institutet, Department of Medical Biochemistry and Biophysics. CPCF is node of the Chemical Proteomics and Proteogenomics Facility at SciLifeLab and of the Swedish national infrastructure for biological mass spectrometry (BioMS) supported by the Swedish Research Council (Vetenskapsrådet). As a method development in CPCF, this work was funded by Science for Life Laboratory, Vetenskapsrådet and Karolinska Institutet.

■ ABBREVIATIONS

5-FU, 5-fluorouracil; ACN, acetonitrile; EPPS, 4-(2-hydroxyethyl)-1-piperazinepropanesulfonic acid; ERF, error function; FA, formic acid; HCD, high energy collision dissociation; HPLC-ESI, high performance liquid chromatography-electrospray ionization; LC−MS/MS, liquid chromatography tandem spectrometry; MS, mass spectrometry; MS/MS, tandem mass spectrometry; MTX, methotrexate; OPLS-DA, orthogonal partial least-squares-discriminant analysis; PBS, phosphate buffer saline; TPP, thermal proteome profiling; TMT, tandem mass tag; SQRT, square root function; UPLC, ultrahigh performance liquid chromatography

■ REFERENCES

(1) Savitski, M. M.; Reinhard, F. B.; Franken, H.; Werner, T.; Savitski, M. F.; Eberhard, D.; Martinez Molina, D.; Jafari, R.; Dovega, R. B.; Klaeger, S.; Kuster, B.; Nordlund, P.; Bantscheff, M.; Drewes, G. Tracking cancer drugs in living cells by thermal profiling of the proteome. *Science* **2014**, *346* (6205), 1255784.

(2) Lomenick, B.; Hao, R.; Jonai, N.; Chin, R. M.; Aghajan, M.; Warburton, S.; Wang, J.; Wu, R. P.; Gomez, F.; Loo, J. A.; Wohlschlegel, J. A.; Vondriska, T. M.; Pelletier, J.; Herschman, H. R.; Clardy, J.; Clarke, C. F.; Huang, J. Target identification using drug affinity responsive target stability (DARTS). *Proc. Natl. Acad. Sci. U. S. A.* **2009**, *106* (51), 21984−9.

(3) Piazza, I.; Kochanowski, K.; Cappelletti, V.; Fuhrer, T.; Noor, E.; Sauer, U.; Picotti, P. A Map of Protein-Metabolite Interactions Reveals Principles of Chemical Communication. *Cell* **2018**, *172* (1−2), 358−372 e23. .

(4) Park, C.; Marqusee, S. Pulse proteolysis: a simple method for quantitative determination of protein stability and ligand binding. *Nat. Methods* **2005**, *2* (3), 207−12.

(5) Vedadi, M.; Niesen, F. H.; Allali-Hassani, A.; Fedorov, O. Y.; Finerty, P. J., Jr.; Wasney, G. A.; Yeung, R.; Arrowsmith, C.; Ball, L. J.; Berglund, H.; Hui, R.; Marsden, B. D.; Nordlund, P.; Sundstrom, M.; Weigelt, J.; Edwards, A. M. Chemical screening methods to identify ligands that promote protein stability, protein crystallization, and structure determination. *Proc. Natl. Acad. Sci. U. S. A.* **2006**, *103* (43), 15835−40.

(6) Becher, I.; Werner, T.; Doce, C.; Zaal, E. A.; Togel, I.; Khan, C. A.; Rueger, A.; Muelbaier, M.; Salzer, E.; Berkers, C. R.; Fitzpatrick, P. F.; Bantscheff, M.; Savitski, M. M. Thermal profiling reveals phenylalanine hydroxylase as an off-target of panobinostat. *Nat. Chem. Biol.* **2016**, *12* (11), 908−910.

(7) Dart, M. L.; Machleidt, T.; Jost, E.; Schwinn, M. K.; Robers, M. B.; Shi, C.; Kirkland, T. A.; Killoran, M. P.; Wilkinson, J. M.; Hartnett, J. R.; Zimmerman, K.; Wood, K. V. Homogeneous Assay for Target Engagement Utilizing Bioluminescent Thermal Shift. *ACS Med. Chem. Lett.* **2018**, *9* (6), 546−551.

DOI: 10.1021/acs.jproteome.9b00500
J. Proteome Res. 2019, 18, 4027−4037

(8) Becher, I.; Andres-Pons, A.; Romanov, N.; Stein, F.; Schramm, M.; Baudin, F.; Helm, D.; Kurzawa, N.; Mateus, A.; Mackmull, M. T.; Typas, A.; Muller, C. W.; Bork, P.; Beck, M.; Savitski, M. M. Pervasive Protein Thermal Stability Variation during the Cell Cycle. *Cell* **2018**, *173* (6), 1495−1507 e18. .
(9) Dai, L.; Zhao, T.; Bisteau, X.; Sun, W.; Prabhu, N.; Lim, Y. T.; Sobota, R. M.; Kaldis, P.; Nordlund, P. Modulation of Protein-Interaction States through the Cell Cycle. *Cell* **2018**, *173* (6), 1481−1494 e13. .
(10) Huber, K. V.; Olek, K. M.; Muller, A. C.; Tan, C. S.; Bennett, K. L.; Colinge, J.; Superti-Furga, G. Proteome-wide drug and metabolite interaction mapping by thermal-stability profiling. *Nat. Methods* **2015**, *12* (11), 1055−7.
(11) Saei, A. A.; Astorga Wells, J.; Sabatier, P.; Beusch, C.; Chernobrovkin, A.; Rodin, S.; Nareoja, K.; Thorsell, A.-G.; Karlberg, T.; Cheng, Q.; Vegvari, A.; Arner, E. S. J.; Schuler, H.; Zubarev, R., System-wide Identification of Enzyme Substrates by Thermal Analysis (SIESTA). *bioRxiv* **2018**.
(12) Molina, D. M.; Jafari, R.; Ignatushchenko, M.; Seki, T.; Larsson, E. A.; Dan, C.; Sreekumar, L.; Cao, Y.; Nordlund, P. Monitoring drug target engagement in cells and tissues using the cellular thermal shift assay. *Science* **2013**, *341* (6141), 84−7.
(13) Lo, M. C.; Aulabaugh, A.; Jin, G.; Cowling, R.; Bard, J.; Malamas, M.; Ellestad, G. Evaluation of fluorescence-based thermal shift assays for hit identification in drug discovery. *Anal. Biochem.* **2004**, *332* (1), 153−9.
(14) Niesen, F. H.; Berglund, H.; Vedadi, M. The use of differential scanning fluorimetry to detect ligand interactions that promote protein stability. *Nat. Protoc.* **2007**, *2* (9), 2212−21.
(15) Bruylants, G.; Wouters, J.; Michaux, C. Differential scanning calorimetry in life science: thermodynamics, stability, molecular recognition and application in drug design. *Curr. Med. Chem.* **2005**, *12* (17), 2011−20.
(16) Brandts, J. F.; Lin, L. N. Study of strong to ultratight protein interactions using differential scanning calorimetry. *Biochemistry* **1990**, *29* (29), 6927−40.
(17) West, G. M.; Thompson, J. W.; Soderblom, E. J.; Dubois, L. G.; Dearmond, P. D.; Moseley, M. A.; Fitzgerald, M. C. Mass spectrometry-based thermal shift assay for protein-ligand binding analysis. *Anal. Chem.* **2010**, *82* (13), 5573−81.
(18) Garbett, N. C.; Mekmaysy, C. S.; Helm, C. W.; Jenson, A. B.; Chaires, J. B. Differential scanning calorimetry of blood plasma for clinical diagnosis and monitoring. *Exp. Mol. Pathol.* **2009**, *86* (3), 186−91.
(19) Massey, A. J. A high content, high throughput cellular thermal stability assay for measuring drug-target engagement in living cells. *PLoS One* **2018**, *13* (4), No. e0195050.
(20) Miettinen, T. P.; Peltier, J.; Hartlova, A.; Gierlinski, M.; Jansen, V. M.; Trost, M.; Bjorklund, M. Thermal proteome profiling of breast cancer cells reveals proteasomal activation by CDK4/6 inhibitor palbociclib. *EMBO J.* **2018**, *37* (10), 1 DOI: 10.15252/embj.201798359.
(21) Park, H.; Ha, J.; Koo, J. Y.; Park, J.; Park, S. B. Label-free target identification using in-gel fluorescence difference via thermal stability shift. *Chem. Sci.* **2017**, *8* (2), 1127−1133.
(22) Turkowsky, D.; Lohmann, P.; Muhlenbrink, M.; Schubert, T.; Adrian, L.; Goris, T.; Jehmlich, N.; von Bergen, M. Thermal proteome profiling allows quantitative assessment of interactions between tetrachloroethene reductive dehalogenase and trichloroethene. *J. Proteomics* **2019**, *192*, 10−17.
(23) Mateus, A.; Maatta, T. A.; Savitski, M. M. Thermal proteome profiling: unbiased assessment of protein state through heat-induced stability changes. *Proteome Sci.* **2016**, *15*, 13.
(24) Volkening, J. D.; Stecker, K. E.; Sussman, M. R. Proteome-wide Analysis of Protein Thermal Stability in the Model Higher Plant Arabidopsis thaliana. *Mol. Cell. Proteomics* **2019**, *18* (2), 308−319.
(25) Mateus, A.; Bobonis, J.; Kurzawa, N.; Stein, F.; Helm, D.; Hevler, J.; Typas, A.; Savitski, M. M. Thermal proteome profiling in bacteria: probing protein state in vivo. *Mol. Syst. Biol.* **2018**, *14* (7), No. e8242.
(26) Sabatier, P.; Saei, A. A.; Wang, S.; Zubarev, R. A. Dynamic Proteomics Reveals High Plasticity of Cellular Proteome: Growth-Related and Drug-Induced Changes in Cancer Cells are Comparable. *Proteomics* **2018**, *18* (24), No. e1800118.
(27) Biltonen, R. L.; Freire, E. Thermodynamic characterization of conformational states of biological macromolecules using differential scanning calorimetry. *Crit. Rev. Biochem.* **1978**, *5* (2), 85−124.
(28) El-Baba, T. J.; Woodall, D. W.; Raab, S. A.; Fuller, D. R.; Laganowsky, A.; Russell, D. H.; Clemmer, D. E. Melting Proteins: Evidence for Multiple Stable Structures upon Thermal Denaturation of Native Ubiquitin from Ion Mobility Spectrometry-Mass Spectrometry Measurements. *J. Am. Chem. Soc.* **2017**, *139* (18), 6306−6309.
(29) Franken, H.; Mathieson, T.; Childs, D.; Sweetman, G. M.; Werner, T.; Togel, I.; Doce, C.; Gade, S.; Bantscheff, M.; Drewes, G.; Reinhard, F. B.; Huber, W.; Savitski, M. M. Thermal proteome profiling for unbiased identification of direct and indirect drug targets using multiplexed quantitative mass spectrometry. *Nat. Protoc.* **2015**, *10* (10), 1567−93.
(30) Childs, D.; Bach, K.; Franken, H.; Anders, S.; Kurzawa, N.; Bantscheff, M.; Mikhail, S.; Huber, W., Non-Parametric Analysis of Thermal Proteome Profiles Reveals Novel Drug-Binding Proteins. *bioRxiv* **2018**.
(31) Cox, J.; Mann, M. MaxQuant enables high peptide identification rates, individualized p.p.b.-range mass accuracies and proteome-wide protein quantification. *Nat. Biotechnol.* **2008**, *26* (12), 1367−72.
(32) Perez-Riverol, Y.; Csordas, A.; Bai, J.; Bernal-Llinares, M.; Hewapathirana, S.; Kundu, D. J.; Inuganti, A.; Griss, J.; Mayer, G.; Eisenacher, M.; Perez, E.; Uszkoreit, J.; Pfeuffer, J.; Sachsenberg, T.; Yilmaz, S.; Tiwary, S.; Cox, J.; Audain, E.; Walzer, M.; Jarnuczak, A. F.; Ternent, T.; Brazma, A.; Vizcaino, J. A. The PRIDE database and related tools and resources in 2019: improving support for quantification data. *Nucleic Acids Res.* **2019**, *47* (D1), D442−D450.
(33) Seashore-Ludlow, B.; Lundback, T. Early Perspective. *J. Biomol. Screening* **2016**, *21* (10), 1019−1033.
(34) Budnik, B.; Levy, E.; Slavov, N. Mass-spectrometry of single mammalian cells quantifies proteome heterogeneity during cell differentiation. *bioRxiv* **2017**, 102681.
(35) Marin-Vicente, C.; Lyutvinskiy, Y.; Romans Fuertes, P.; Zubarev, R. A.; Visa, N. The effects of 5-fluorouracil on the proteome of colon cancer cells. *J. Proteome Res.* **2013**, *12* (4), 1969−79.
(36) Qiu, Q.; Huang, J.; Shu, X.; Fan, H.; Zhou, Y.; Xiao, C. Polymorphisms and Pharmacogenomics for the Clinical Efficacy of Methotrexate in Patients with Rheumatoid Arthritis: A Systematic Review and Meta-analysis. *Sci. Rep.* **2017**, *7*, 44015.
(37) Rajagopalan, P. T.; Zhang, Z.; McCourt, L.; Dwyer, M.; Benkovic, S. J.; Hammes, G. G. Interaction of dihydrofolate reductase with methotrexate: ensemble and single-molecule kinetics. *Proc. Natl. Acad. Sci. U. S. A.* **2002**, *99* (21), 13481−6.
(38) Visentin, M.; Zhao, R.; Goldman, I. D. The antifolates. *Hematol Oncol Clin North Am.* **2012**, *26* (3), 629−48 ix. .
(39) Wyatt, M. D.; Wilson, D. M., 3rd Participation of DNA repair in the response to 5-fluorouracil. *Cell. Mol. Life Sci.* **2009**, *66* (5), 788−99.
(40) Almqvist, H.; Axelsson, H.; Jafari, R.; Dan, C.; Mateus, A.; Haraldsson, M.; Larsson, A.; Martinez Molina, D.; Artursson, P.; Lundback, T.; Nordlund, P. CETSA screening identifies known and novel thymidylate synthase inhibitors and slow intracellular activation of 5-fluorouracil. *Nat. Commun.* **2016**, *7*, 11040.
(41) Jafari, R.; Almqvist, H.; Axelsson, H.; Ignatushchenko, M.; Lundback, T.; Nordlund, P.; Martinez Molina, D. The cellular thermal shift assay for evaluating drug target interactions in cells. *Nat. Protoc.* **2014**, *9* (9), 2100−22.
(42) Chernobrovkin, A.; Marin-Vicente, C.; Visa, N.; Zubarev, R. A. Functional Identification of Target by Expression Proteomics (FITExP) reveals protein targets and highlights mechanisms of action of small molecule drugs. *Sci. Rep.* **2015**, *5*, 11176.

DOI: 10.1021/acs.jproteome.9b00500
J. Proteome Res. 2019, 18, 4027−4037

(43) Longley, D. B.; Harkin, D. P.; Johnston, P. G. 5-fluorouracil: mechanisms of action and clinical strategies. *Nat. Rev. Cancer* **2003**, *3* (5), 330−8.
(44) Danenberg, P. V. Thymidylate synthetase - a target enzyme in cancer chemotherapy. *Biochim. Biophys. Acta, Rev. Cancer* **1977**, *473* (2), 73−92.
(45) Gustavsson, M.; Ronne, H. Evidence that tRNA modifying enzymes are important in vivo targets for 5-fluorouracil in yeast. *RNA* **2008**, *14* (4), 666−74.
(46) Hoang, C.; Hamilton, C. S.; Mueller, E. G.; Ferre-D'Amare, A. R. Precursor complex structure of pseudouridine synthase TruB suggests coupling of active site perturbations to an RNA-sequestering peripheral protein domain. *Protein Sci.* **2005**, *14* (8), 2201−6.
(47) Rintala-Dempsey, A. C.; Kothe, U. Eukaryotic stand-alone pseudouridine synthases - RNA modifying enzymes and emerging regulators of gene expression? *RNA Biol.* **2017**, *14* (9), 1185−1196.
(48) Samuelsson, T. Interactions of transfer RNA pseudouridine synthases with RNAs substituted with fluorouracil. *Nucleic Acids Res.* **1991**, *19* (22), 6139−44.
(49) Zhao, X.; Yu, Y. T. Incorporation of 5-fluorouracil into U2 snRNA blocks pseudouridylation and pre-mRNA splicing in vivo. *Nucleic Acids Res.* **2006**, *35* (2), 550−8.
(50) Saei, A. A.; Sabatier, P.; Tokat, U. G.; Chernobrovkin, A.; Pirmoradian, M.; Zubarev, R. A. Comparative Proteomics of Dying and Surviving Cancer Cells Improves the Identification of Drug Targets and Sheds Light on Cell Life/Death Decisions. *Mol. Cell. Proteomics* **2018**, *17* (6), 1144−1155.
(51) Saei, A. A.; Chernobrovkin, A.; Sabatier, P.; Zhang, B.; Beusch, C.; Tokat, Ü. G.; Gaetani, M.; Végvári, Á.; Zubarev, R. A. ProTargetMiner: A proteome signature library of anticancer molecules for functional discovery. *bioRxiv* **2018**, 421115.
(52) Klaeger, S.; Gohlke, B.; Perrin, J.; Gupta, V.; Heinzlmeir, S.; Helm, D.; Qiao, H.; Bergamini, G.; Handa, H.; Savitski, M. M.; Bantscheff, M.; Medard, G.; Preissner, R.; Kuster, B. Chemical Proteomics Reveals Ferrochelatase as a Common Off-target of Kinase Inhibitors. *ACS Chem. Biol.* **2016**, *11* (5), 1245−54.
(53) Leuenberger, P.; Ganscha, S.; Kahraman, A.; Cappelletti, V.; Boersema, P. J.; von Mering, C.; Claassen, M.; Picotti, P. Cell-wide analysis of protein thermal unfolding reveals determinants of thermostability. *Science* **2017**, *355* (6327), eaai7825.

DOI: 10.1021/acs.jproteome.9b00500
J. Proteome Res. 2019, 18, 4027−4037